Journal of Hydrology, 153 (1994) 339–355
0022-1694/94/$07.00

[1]

Some Eulerian and Lagrangian statistical properties of rainfall at small space–time scales

Ronny Berndtsson*[,a], Kenji Jinno[a], Akira Kawamura[a], Magnus Larson[b], Janusz Niemczynowicz[b]

[a]*Department of Civil Engineering (Suiko), Kyushu University, Fukuoka, Japan*
[b]*Department of Water Resources Engineering, University of Lund, Lund, Sweden*

(Received 15 April 1992; revision accepted 21 May 1993)

Abstract

Management of urban hydrological systems requires a knowledge of short-term and small-scale rainfall properties. Small catchment areas, dense building structures, a high degree of impermeable areas, and resulting rapid runoff, mean that the properties of individual rain cells are important considerations. Accordingly, this paper characterizes mainly spatial rainfall properties on a scale suitable for urban hydrology. Because of the usually dominant advective velocity component of individual rain cells the Eulerian view (observations of the moving rain cell by a fixed rain gage network) gives a distorted picture in the direction of movement of the actual rain cell. The extent of distortion depends on the magnitude of the advective velocity. The Lagrangian approach (moving along with the same speed and direction as the cell) gives different information regarding cell characteristics (e.g. size) compared with the Eulerian approach. It is shown that the Lagrangian cell size as indicated by the spatial correlation structure on average is twice the size of the Eulerian cell size. Thus, it is argued that the Lagrangian approach provides a more realistic picture of the rainfall structures compared with the Eulerian approach. The cell properties exhibit a temporal persistence of the spatial characteristics in the direction of movement. This persistence is, however, not strong and thus a forecasting procedure using advection only does not seem appropriate.

1. Introduction

Water management in both rural and urban areas is based on a detailed knowledge of spatial and temporal rainfall variability. A problem area that is often overlooked, or even neglected, in fundamental research on rainfall, however, is urban hydrology or urban hydrological management. A factor that has hampered urban hydrology from becoming more of a science is a lack of knowledge of physical processes that govern rainfall and runoff

* Corresponding author.

SSDI 0022-1694(93)02383-9

characteristics at small space–time scales that are important for urban catchments. This is to a major extent caused by the extreme scarcity of detailed historical data (e.g. Chan and Bras, 1979). Compared with rural areas, hourly rainfall data are too crude for urban catchment areas with a typical size of 1–2 km^2 (Schilling, 1990). In most of these catchments the overland flow time to gutter inlets is seldom longer than 1–10 min. The flow time in a single drain pipe or sewer is usually between 1 and 5 min. This leads to special requirements concerning the rainfall observations used in, for example, runoff routing (Yen, 1987; Messaoud and Pointin, 1990). Consequently, in real-time prediction of runoff in urban areas detailed knowledge is needed on the smallest rainfall structures, i.e. individual convective cells. These cells typically have an area of 2–10 km^2 (e.g. Niemczynowicz and Jönsson, 1981; Berndtsson and Niemczynowicz, 1986), are highly dynamic, and undergo different development stages during a few minutes (Hobbs and Locatelli, 1978).

The main objectives of this paper are: (1) to introduce a new method to statistically characterize short-term rainfall data collected by rain gages, and (2) to present mainly spatial rainfall properties on a scale suitable for real-time prediction in urban areas. The paper forms the basis for a modeling approach in a related paper (Jinno et al., 1993). For this purpose, the first part of the paper presents a statistical analysis using both the Lagrangian and Eulerian approaches applied to ten high-intensive rainfall events. The second part gives information on the bulk properties of rainfall data collected during 3 years. The results can be used for rainfall interpolation procedures and the design of urban rainfall data collection systems.

2. Experimental layout

The experimental rain gage network is located in the city of Lund (about 70 000 inhabitants) in southern Sweden. The winters are usually mild with an average temperature around 0°C and the summers have an average temperature of about 20°C. The mean annual rainfall is approximately 650 mm and the dominant mechanism for rainfall generation is passage of large-scale frontal systems. During late summer (July–August), however, intensive local convective storms also contribute significantly to the annual total precipitation (Niemczynowicz and Jönsson, 1981). The topography of the gaged area is predominantly flat but with a marked gradient from southwest to northeast (increasing from 20 to 70 m a.m.s.l.). This is reflected in an increasing annual precipitation from the southwest to the northeast (about 35 mm $year^{-1}$ km^{-1}).

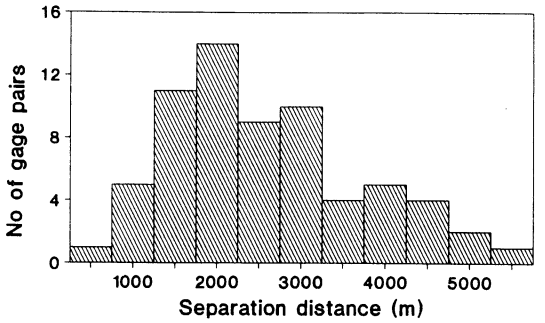

Fig. 1. Distribution of separation distances between gages for all gage pairs (in total 66).

Twelve rain gages covered the main part of the city (25 km^2) during a 3 year observation period (1979–1981; see Niemczynowicz, 1984). The average distance between gages (in total 66 intergage distance combinations) was 2.6 km, whereas the minimum and maximum distances were 0.7 km and 5.6 km, respectively (Figs. 1 and 2). The gages were of the tipping-bucket type with an average of 0.035 mm per tipping, and the number of tippings was recorded at 1 min intervals. All gages functioned automatically and were connected to a central recording unit that allowed for synchronous observations. Further details on the operation of the network and calibration procedures for the tipping-bucket gages are described by Niemczynowicz (1984) and Niemczynowicz and Dahlblom (1984).

3. General properties of urban-scale rainfall

Current research on spatial rainfall dynamics has emphasized mesoscale properties according to the terminology of Orlanski (1975) (e.g. Gupta and Waymire, 1979; Gupta, 1985). For subsynoptic precipitation fields it is the convective cells that are of main interest in urban hydrology. However, small mesoscale areas also need to be considered since these may contribute a lower and spatially more uniform rainfall intensity embedding the individual rain cells.

The individual convective rain cells typically undergo three different development stages: (1) the cumulus stage; (2) the mature stage; (3) the dissipating stage (Hobbs and Locatelli, 1978; Gupta and Waymire, 1979). The pioneering observations on subsynoptic rainfall features made by Austin and Houze (1972) were mainly from cyclonic storms. However, air-mass thunderstorms also display similar characteristics but without synoptic areas; they consist of isolated convective cells or clusters of cells (Gupta and Waymire, 1979). The physical background governing the dynamics of the subsynoptic elements, however, has been little investigated (Cho, 1985; Berndtsson and Niemczynowicz, 1988).

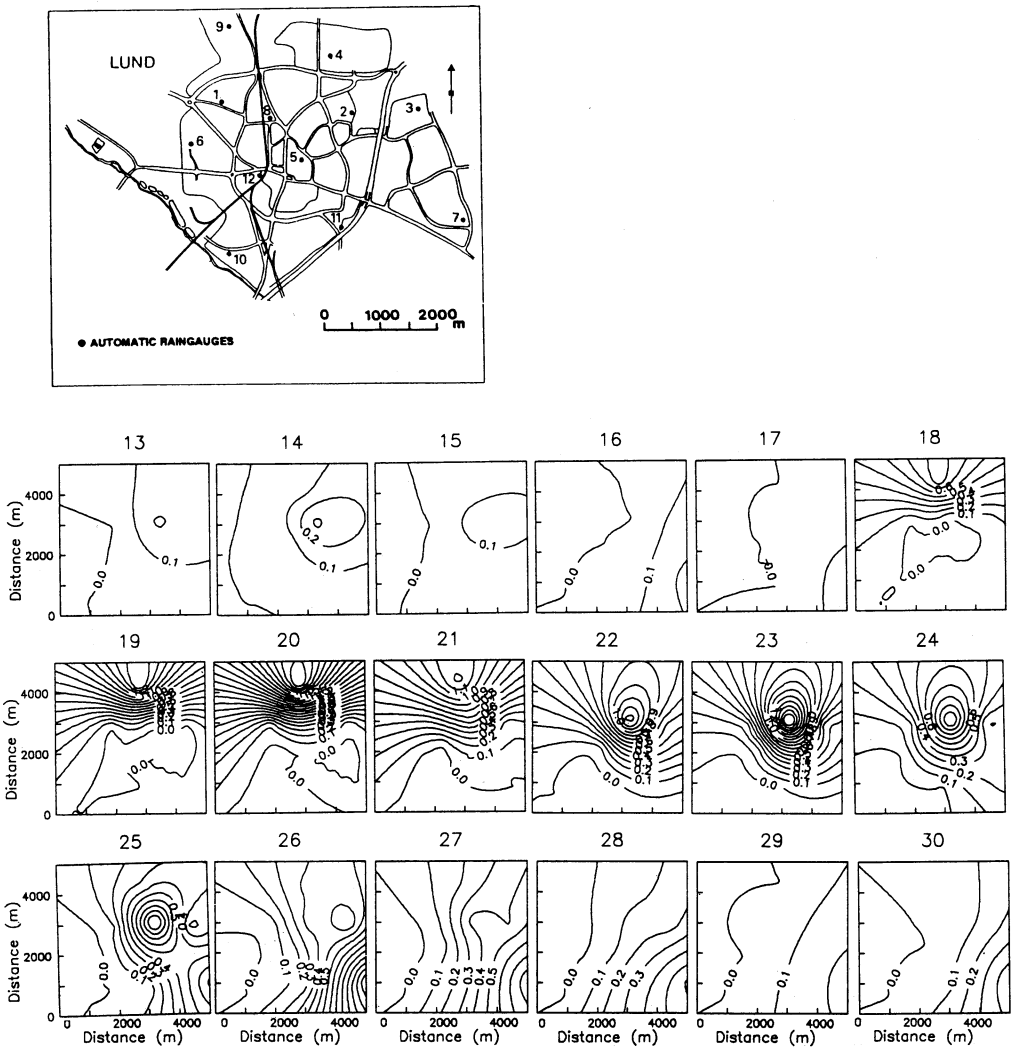

Fig. 2. Rain gage location and the temporal evolution of a cell-shaped rainfall structure over the network during 18 min (time step 13–30; event 23 August 1980 (mm min^{-1})).

Gupta and Waymire (1979) concluded that convective rain cells have an areal extent of about 10–30 km^2, and a life-span from several minutes to about 1 h. However, several recent studies indicate that the areal extent of a cell may be much smaller (Marshall, 1980; Niemczynowicz and Jönsson, 1981; Shaw, 1983; Berndtsson and Niemczynowicz, 1986; Crane, 1990). This is especially true for rainfall associated with individual convective cells emanating from thunderstorms, downburst or microburst phenomena. Browning and Collier (1989) indicated that the time scale for validity of extrapolation of

microbursts may be one to a few minutes which indicates a very limited areal extent. Examples of the size of individual rain cells as observed by rain gages have been given, e.g. in Lund by Niemczynowicz and Jönsson (1981), in semiarid Tunisia by Berndtsson and Niemczynowicz (1986), in Great Britain by Felgate and Read (1975), Marshall (1980), and Shaw (1983), in Israel by Sharon (1972), and in the United States by Hershfield (1962), Huff and Shipp (1969), and others. It appears that the size of the reported individual rain cells decreases in proportion to the temporal and spatial resolution of the observation network, i.e. denser networks detect smaller cells.

Figure 2 shows minute time series of the spatial rainfall distribution as a cell-shaped rainfall structure moves in over the rain gage network in Lund. Observations from ten gages were used for the interpolation between gages. From time step 18 a clear cell-shaped structure is seen in the diagrams. The cell moves gradually from north to southeast. The speed and the direction of movement of the cell can be calculated approximately to be 8–9 m s^{-1} by comparing the locations of the cell center at different times. Below we outline a more general procedure for characterizing the spatial behavior of moving cells.

4. Methodological considerations

An approach to studying moving rain cells was delineated by Marshall (1980) and Niemczynowicz and Jönsson (1981). The method can be used to display shape, size, and movement of a statistically defined rain cell structure using rain gage data. The method involves calculation of cross-correlation coefficients between different gages for time series with consecutive temporal lags. In this paper we refer to the results of this method as Eulerian space–time correlation fields. By this we mean that the moving rain cells are observed at fixed ground locations (rain gages) and, thus, the denotation Eulerian. As the moving rain cell is observed by a fixed rain gage system on the ground the cell will appear contracted in the direction of movement. This contraction or distortion will increase as the speed of the rain cell increases.

The Eulerian space–time correlation field γ_E for the rainfall intensity field R is defined as

$$\gamma_E(\boldsymbol{\xi}, \tau) = \mathrm{Corr}[R(\mathbf{x}, t), R(\mathbf{x} + \boldsymbol{\xi}, t + \tau)] \quad (1)$$

where t is time, $\mathbf{x}$ is a space vector, $\boldsymbol{\xi}$ is a vector representing the distance in space between gaging points, and τ is the time lag.

The Eulerian space–time correlation field γ_E has to be estimated from the existing rain gage network, which in the present study means 12 gages. Therefore, γ_E is approximated by use of a correlation matrix $\mathbf{M}\gamma(\mathbf{x}_i,\mathbf{x}_j,\tau)$

according to

$$\gamma_E(\boldsymbol{\xi}, \tau) \approx \mathbf{M}\gamma(\mathbf{x}_i, \mathbf{x}_j, \tau) \tag{2}$$

The correlation matrix $\mathbf{M}\gamma(\mathbf{x}_i, \mathbf{x}_j, \tau)$ contains correlation coefficients according to

$$\mathbf{M}_\gamma(\mathbf{x}_i, \mathbf{x}_j, \tau) = \begin{vmatrix} 1 & \gamma(\mathbf{x}_1, \mathbf{x}_2, \tau) & \gamma(\mathbf{x}_1, \mathbf{x}_3, \tau) & \dots & \gamma(\mathbf{x}_1, \mathbf{x}_n, \tau) \\ \gamma(\mathbf{x}_2, \mathbf{x}_1, \tau) & 1 & \gamma(\mathbf{x}_2, \mathbf{x}_3, \tau) & \dots & \gamma(\mathbf{x}_2, \mathbf{x}_n, \tau) \\ \gamma(\mathbf{x}_3, \mathbf{x}_1, \tau) & . & 1 & \dots & \\ . & . & . & . 1 & \dots \\ . & . & . & . & . 1 \quad \dots \\ . & . & . & . & . \; . \quad 1 \quad \dots \\ \gamma(\mathbf{x}_{n-1}, \mathbf{x}_1, \tau) & \gamma(\mathbf{x}_{n-1}, \mathbf{x}_2, \tau) & \dots & \gamma(\mathbf{x}_{n-1}, \mathbf{x}_n, \tau) & 1 \end{vmatrix} \tag{3}$$

where $\gamma(\mathbf{x}_i,\mathbf{x}_j,\tau)$ correlation coefficients for time lag τ calculated from gage pairs $\mathbf{x}_i$ and $\mathbf{x}_j$. In total there are $n(n-1)$ gage combinations where n is the number of gages in the network. The correlation $\gamma(\mathbf{x}_i,\mathbf{x}_j,\tau)$ between gages $\mathbf{x}_i$ and $\mathbf{x}_j$ for time series of rainfall is calculated as

$$\gamma(\mathbf{x}_i, \mathbf{x}_j, \tau) = \frac{\mathrm{cov}[R(\mathbf{x}_i, t), R(\mathbf{x}_j, t+\tau)]}{\mathrm{var}[R(\mathbf{x}_i, t)]\mathrm{var}[R(\mathbf{x}_j, t+\tau)]^{1/2}} \tag{4}$$

where $R(\mathbf{x}_i, t)$ is rainfall at gage $\mathbf{x}_i$ for time t and $R(\mathbf{x}_j, t+\tau)$ is rainfall at gage $\mathbf{x}_j$ for time $t+\tau$.

If second-order stationarity (both mean and covariance are independent of spatial location) is assumed for the observations, the correlation can be expressed in a general way as a function of distance h and direction ϕ only according to

$$\gamma(h, \phi, \tau) = \gamma(\mathbf{x}_i, \mathbf{x}_j, \tau) \tag{5}$$

The correlation $\gamma(h,\phi,\tau)$ may be plotted either, depending on distance only, or depending on both distance and direction. If the spatial correlation function is isotropic in all directions the correlation–distance diagram contains all necessary information. Otherwise, the correlation function is non-isotropic and directional information needs to be included. Sharon (1974) used the notation composite correlation maps to plot the correlation $\gamma(h,\phi,\tau)$ in a single diagram. In the present paper we use $\mathbf{M}\gamma(\mathbf{x}_i,\mathbf{x}_j,\tau)$ to interpolate the $\gamma(h,\phi,\tau)$ function in space.

As discussed above an Eulerian view gives a distorted picture of the rainfall field because of the rain cell movement in relation to the fixed observation system. Therefore, Lagrangian (moving along with the same speed as the cell)

correlation fields were also calculated. The Lagrangian correlation field for an individual rain cell is defined as

$$\gamma_L(\tau) = \mathrm{Corr}[R(t), R(t+\tau)] \tag{6}$$

However, since we do not have any observation system with its origin in the cell center that is moving along with the same speed and direction as the rain cells (observation system with Lagrangian coordinates), the Eulerian observations were used to estimate the Lagrangian correlation fields. Here it was assumed that the 'frozen flow field hypothesis' of Taylor (1938) is valid. This hypothesis allows the determination of spatial correlations from temporal correlations under the assumption that the turbulent eddies are advected past the point of observation by the mean flow so fast that they do not change substantially during their time of passage. The work of Zawadzki (1973) indicates that this hypothesis is valid for convective rainfall fields for time periods shorter than 40 min but not for longer periods. Since this study is concerned with time periods typically less than 10 min this assumption seems to be well justified. Hence, we may define an advective velocity u_c at which turbulent eddies are advected by the mean flow assuming that the turbulence is stationary in time and homogeneous in the direction of movement (e.g. Panofsky and Dutton, 1984) so that

$$|\boldsymbol{\xi}| = u_c \tau \tag{7}$$

Thus, the Lagrangian correlation fields may be estimated from the Eulerian correlation fields as (substitution of Eq. (7) into Eq. (1))

$$\gamma_L^*(\tau) = \gamma_E(\boldsymbol{\xi}, |\boldsymbol{\xi}|/u_c) \tag{8}$$

Since the observation network only consists of 12 gages the estimation of u_c is difficult due to there being few observation points. Thus, the Lagrangian correlation coefficients were estimated as the lag-τ coefficients that maximized Eq. (4) for each gage combination according to (e.g. Zawadzki, 1973)

$$\gamma_L^*(\tau) \approx \max[\gamma(\mathbf{x}_i, \mathbf{x}_j, \tau)] \tag{9}$$

Therefore, it is assumed that the rain gage combination that displays a maximum correlation for a specific temporal lag will be in the direction of the mean velocity component according to Eq. (7).

To compare the Eulerian and Lagrangian rain cell properties on a more general basis, the sizes of the Eulerian and Lagrangian correlation fields were calculated. The sizes of the Eulerian correlation fields within the 0.5 correlation isoline was calculated according to

$$\Gamma_E(\tau) = \int \gamma_E(\boldsymbol{\xi}, \tau) \mathrm{d}\xi \quad [\gamma_E(\boldsymbol{\xi}, \tau) \geqslant 0.5] \tag{10}$$

The corresponding size of the Lagrangian correlation fields was calculated as

$$\Gamma_L = \int \gamma_E(\boldsymbol{\xi}, |\boldsymbol{\xi}|/u_c)\mathrm{d}\xi, \quad [\gamma_E(\boldsymbol{\xi}, |\boldsymbol{\xi}|u_c) \geqslant 0.5] \tag{11}$$

5. Dynamic properties of individual rain cells

The ten most high-intensive rainfall events during the 3 year observation period were investigated by calculating the Eulerian and Lagrangian correlation fields according to the theoretical methodology above. The maximum point value intensities for these events varied from 1.5 to 2.5 mm min^{-1}. The events with the highest intensities represented rainfall intensities with a return period of 5–10 years (Niemczynowicz and Jönsson, 1981). Figure 3 shows an example of the dynamic behavior of one of the most high-intensive 1 h rainfall events (23 August 1980 10:55–11:54h) recorded during the 3 year measurement period (see Fig. 2). The maximum 1 min intensity was 2.25 mm min^{-1}. The figure shows Eulerian correlation isolines of 0.4 and above for different temporal lags τ. A well-defined correlation structure moves with a significant speed from the center to the southeast corner of the gaging network during about 8 min (from $\tau = 0$–8). The presence of two intensity peaks is indicated in the correlation fields. The cell structure gradually develops as indicated by an increase in correlation, then dissipates (decreasing correlation but increasing area), and eventually disappears. By calculating the movement of the center of gravity, the speed was estimated to be about 10 m s^{-1}.

In the case above, the time evolutions of the Eulerian correlation fields were shown during a portion of a rainfall event. However, since the rain cells may move with a predominant speed in relation to the fixed observation network a distorted representation of the cell shapes is obtained in the direction of movement. The distortion depends on the speed and will make the cell look contracted in the direction of movement. The higher the cell speed is, the more contracted the cell will look like at the fixed network.

In total about 400 rainfall events were identified during the observation period (events defined as separated by at least a 15 min period of no rainfall recording and with an intensity exceeding 3.3 mm per 10 min; Niemczynowicz, 1984). The average speed for all cells identified during these events was 10.4 m s^{-1}. This implies that individual rain cells may pass over an average-sized urban catchment with a typical length-scale of 1.5 km during about 2–3 min and over an average-sized city (typical length-scale of 5 km) in less than 10 min.

Figure 4 shows an example of estimated Lagrangian correlation by Eq. (9) depending on the parameters τ and $\boldsymbol{\xi}$ in Eq. (7) for rainfall event 23 August

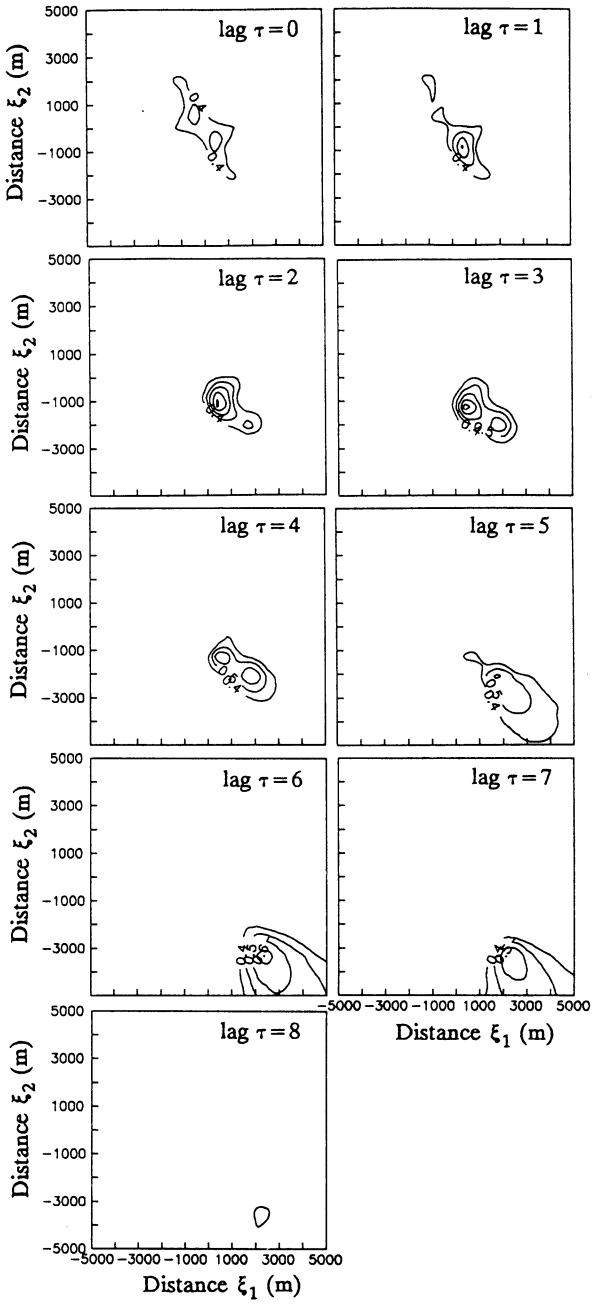

Fig. 3. Eulerian correlation fields $\gamma_E(\xi,\tau)$ for $\tau = 0$–8 min showing the shape, size, and movement of a rain cell (event 23 August 1980 10:55–11:54 h; 1 min data).

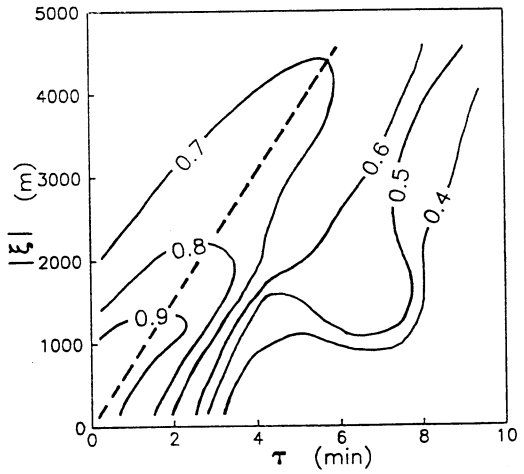

Fig. 4. Lagrangian correlation $\gamma_L^*(\tau) \approx \max[\gamma(\mathbf{x}_i, \mathbf{x}_j, \tau)]$ depending on parameters τ and ξ in Eq. (7) for event 23 August 1980 10:04–11:03 h. The broken line is used to estimate the average velocity of the rain cell (about 12.5 m s^{-1}).

1980 10:04–11:03 h (1 min data). The correlation displays a fairly consistent linear structure from which u_c can be estimated (the broken line in the figure) to about 12.5 m s^{-1}. Figure 4 can be used to assess the performance of a prediction procedure based on pure translation (prediction by advection only) of the observed rain cell. It is seen that the spatial rainfall structure as observed from 1 min data displays a temporal persistence in the direction of movement (in this case a correlation of about 0.7 up to a time lag of 6 min and a distance of 4.5 km). This means that a correlation of about 0.7 between predicted and actual rainfall can be expected for a prediction period of 6 min when the prediction technique is based on a frozen rainfall pattern that is being moved in the general direction of movement (pure advection). Only for very short prediction periods like 2 min and a distance of about 1 km can a high correlation (0.9) be expected between predicted and observed rainfall using the translation technique.

Figure 5 shows the Lagrangian correlation field corresponding to the Eulerian correlation fields in Fig. 3. It is seen that there is a great difference between the two types of structures. The size of the Lagrangian structure is several times larger as compared with the size found by the Eulerian approach. As expected the spatial distortion is greatest in the direction of movement (northwest–southeast). This means that the rainfall structure, i.e. as interpreted by the Lagrangian approach, seems to be distorted several times owing to its speed when observed by the fixed rain gage network. It should be noted that the Lagrangian structure should be interpreted as the average

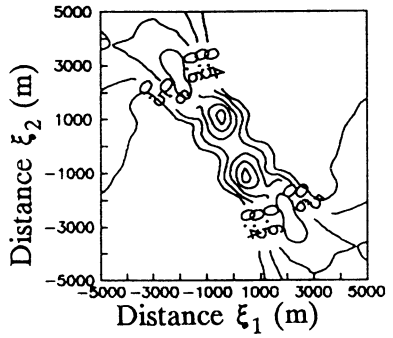

Fig. 5. Lagrangian correlation fields $\gamma_L^*(\tau)$ showing actual shape and size of the rain cell in Fig. 3.

size and shape during the investigated time frame while the Eulerian structure gives information at several time lags during the time frame.

Since the feasibility of short-term rainfall forecasting for small spatial scales mainly depends on the time aggregation and forecasting period the 1 min data were aggregated into time intervals of 2–5 min, and then analyzed with the above correlation technique. Figure 6 shows the results of these calculations expressed as mean values of the area delimited by the 0.5 correlation isoline according to Eqs. (10) and (11) for the ten events studied. It can be seen that the Lagrangian correlation areas are generally at least double the size of the corresponding Eulerian correlation areas. The sizes of the Eulerian correlation areas depending on lag time show that the rainfall structures undergo rapid spatial changes which in turn mean a low forecasting possibility. A priori one would assume that aggregation of data in time would increase the spatial dependence. This is also the case for $\tau = 0$ and $\tau = 1$ (time lag 0 and time lag 1 correlation areas), however, for larger time lags the aggregation results in decreasing Eulerian correlation areas. The Lagrangian correlation areas, however, appear to increase in size up to about 65 km^2 for a 3 min

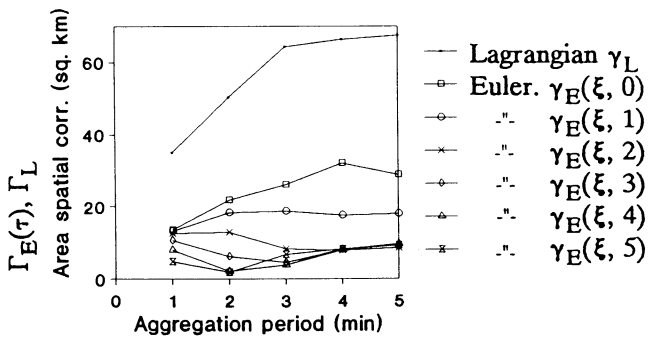

Fig. 6. Comparison of average Eulerian and Lagrangian correlation fields for the ten most high-intensive 1 h rainfall events during the observation period aggregated into different time periods (areas within the 0.5 correlation isoline; the time lag is 0–5 min).

aggregation period. For larger aggregation periods (3–5 min) the areas appear to be almost constant. This may be interpreted as an actual increase in the rain cell area for aggregations up to about 3 min, an increase that is disguised to the Eulerian observer.

Figure 6 shows to what extent the advective behavior of rainfall cells influences the result of Eulerian observations at ground level. From the figure it is inferred, for example, that the cell size that is interpreted from the fixed rain gage network (Eulerian approach) may be very different from the cell size interpreted from the advective movement (Lagrangian approach) of the cells. This may explain differences in rain gage and radar observations and the difference in reported cell size for different gaging networks. The figure can also be used to obtain a general picture of the rainfall area that may be possible to forecast and how this area changes in size depending on time lag and aggregation period.

Since the method described above uses the correlation coefficient to describe the space–time dependence structure of rainfall variability it may also be used to give a statistical measure of the uncertainty of each calculated coefficient. In the presented diagrams of space–time correlation fields, correlation coefficients were generally based on 60 individual values. This results in an overall rather high statistical significance even for small correlation coefficients (under the assumption of normality, correlation coefficients equal to about 0.25 are statistically different from zero at the 95% probability level; Yevjevich, 1972). Even so, since the analyses are based exclusively on higher correlation coefficients (above 0.4) and since the space–time correlation fields are the results of simultaneous observations from many spatial points it is believed that displayed results are far outside the statistical errors in the estimation method. The statistical structures of many simultaneous coefficients and the logical consistency of these structures may be considered significant from a physical viewpoint.

6. Properties of long-term rainfall

The entire 3 year data set was used directly without division into individual events for further statistical analyses of non-dynamic properties of long-term observations. Figure 7 shows an example of Eulerian correlation decay and scatter with intergage distance for three aggregation periods (γ_E $|\xi|$,0); 1 min, 5 min, and 10 min respectively). Correlation coefficients were calculated by excluding aggregated data occurring as zero rainfall at both of the pairwise combined stations. This was done to avoid an apparent increase in correlation as a result of long dry periods (see e.g. Berndtsson, 1987, 1988). On average

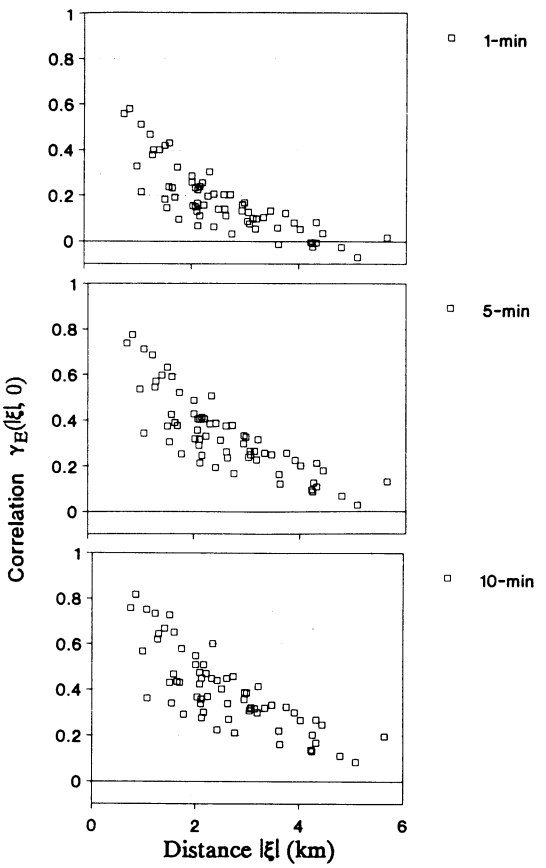

Fig. 7. Examples of time-lag zero correlation coefficients for data aggregated during 1 min, 5 min, and 10 min, respectively, versus interstation distances (data observed during 3 years).

this exclusion lowered the correlation coefficient with a value of about 0.09. From the figure it is seen that the correlation increases gradually for decreasing distances and appears to approach unity at zero distance. Observation errors and small-scale variability (occurring at scales less than 1 km) for the total 3 year data series seem, therefore, to be small. Aggregating the data into longer periods gradually increases the spatial correlation. If the 0.5 correlation level is assumed to represent an acceptable statistical significance level, it is seen that about 500 m is the shortest distance between gages to obtain information about spatial properties for 1 min data.

Figure 8 shows the corresponding Eulerian correlation areas ($\gamma_E|\boldsymbol{\xi}|,0$) for the same three aggregation periods. Figures 7 and 8 do not reveal any properties of individual rainfall cells, but the correlation structure may indicate overall spatial properties of rainfall aggregated to periods and the spatial resolution of rain gage networks needed to detect spatial variability for time

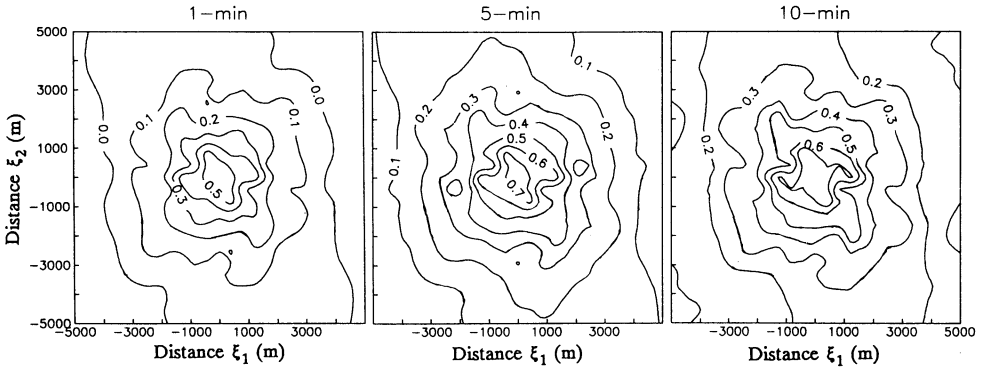

Fig. 8. Eulerian correlation fields $\gamma_E(\xi,0)$ for data aggregated to 1 min, 5 min, and 10 min, respectively (data observed during 3 years).

scales of less than 10 min. It is also seen in Fig. 8 that the correlation fields are not isotropic, but are typically elongated in the north–northwest and south–southeast direction. This may be an influence of preferential storm paths (Niemczynowicz, 1987). The area within the 0.5 correlation isoline increases as the aggregation period increases. For 1 min data this area corresponds to 2.9 km^2. For 5 and 10 min aggregation periods, the areas are 8.2 km^2 and 12.5 km^2, respectively. Thus, to obtain observations with a statistical significance representing 0.5 correlation, the necessary intergage distances can be determined from the radii of the above areas (assuming correlation areas with a circular shape), which are 1.0 km, 1.6 km, and 2.0 km, respectively. These distances may be used when designing urban gaging systems for a specific time resolution.

Figure 9 shows the size of the spatial correlation fields ($\gamma_E|\boldsymbol{\xi}|,\tau$) and $\gamma_L(\tau)\approx \gamma_E(\boldsymbol{\xi},|\boldsymbol{\xi}|/u_c)$) within the 0.5, 0.4, and 0.3 correlation isolines depending on time lag and aggregation period (data observed during 3 years). It is seen that the correlation areas decrease rapidly as the time lag increases from 0 to 3 min. This displays the small temporal persistence of non-dynamic rainfall that is averaged over long periods as opposed to short-term data for individual events. The Lagrangian correlation fields are approximately equal to the size of the Eulerian for $\tau = 0$ (time lag 0 correlation fields), because the directional dependence and dynamics of individual events are averaged out in the long-term data. Figure 9 may be employed to get an overall picture of the necessary spatial resolution of rain gage networks for rainfall sampled during different aggregation periods. It also provides information on the temporal persistence of rainfall with respect to different aggregation periods. This kind of information may be needed in temporal rainfall models.

When calculating correlation coefficients for the entire observation period (3 years) and using 1–10 min data, the statistical significance is high even for small correlation coefficients. This depends on the large

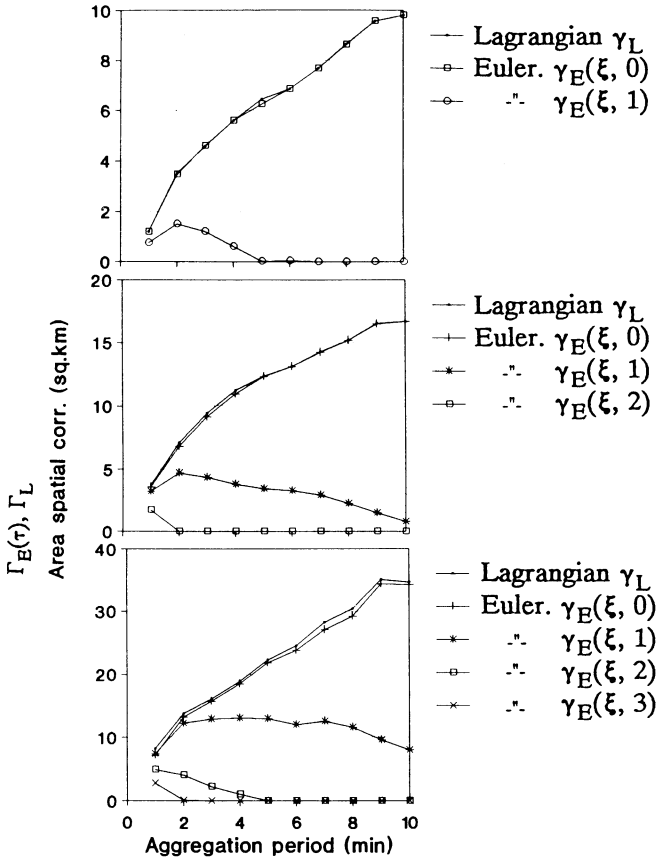

Fig. 9. Size of spatial correlation fields within the 0.3, 0.4, and 0.5 correlation isolines depending on time lag and aggregation period (1–10 min data observed during 3 years; the time lag is 0–3 min).

amount of values used in the calculation (1 min data for 3 years). In most cases, a correlation coefficient around 0.1 would be significantly different from zero on the 95% probability level. However, as discussed above, the diagrams are not based on individual coefficients but instead on consistent patterns using 66 simultaneous combinations ($n(n-1)/2$). This is why errors and uncertainties in individual coefficients may be smoothed out.

7. Summary and discussion

Because of the usually dominant advective velocity component of individual rain cells the Eulerian view gives a distorted picture in the direction of movement of the actual rainfall cell. The extent of distortion depends on the magnitude of the advective velocity. The Lagrangian approach (moving with the cell at a specific speed and direction) gives larger correlation areas within a

chosen isoline compared with the Eulerian approach (observing moving rain cells at fixed ground locations). This indicates that the Lagrangian approach provides a more realistic picture of the rainfall structures compared with the Eulerian approach.

Figure 4 shows that there is a persistence in time of spatial cell properties in the direction of movement. This persistence is, however, not strong (as seen from rapidly decreasing correlation with time and space lag) and, thus, a forecasting procedure using advection only does not seem appropriate.

Acknowledgments

This research was in part supported by the Japan Society for the Promotion of Science and the Japanese Ministry of Education by giving one of the authors (RB) the chance to spend a sabbatical year at Kyushu University. Part of the support came from the Swedish Natural Science Research Council. This support is gratefully acknowledged.

References

Austin, P.M. and Houze, R.A., 1972. Analysis of the structure of precipitation patterns in New England. J. Appl. Meteorol., 11: 926–934.

Berndtsson, R., 1987. On the use of cross-correlation analysis in studies of patterns of rainfall variability. J. Hydrol., 93: 113–134.

Berndtsson, R., 1988. Temporal variability in spatial correlation of daily rainfall. Water Resour. Res., 24: 1511–1517.

Berndtsson, R. and Niemczynowicz, J., 1986. Spatial and temporal characteristics of high-intensive rainfall in northern Tunisia. J. Hydrol., 87: 285–298.

Berndtsson, R. and Niemczynowicz, J., 1988. Spatial and temporal scales in rainfall analysis: Some aspects and future perspectives. J. Hydrol., 100: 293–313.

Browning, K.A. and Collier, C.G., 1989. Nowcasting of precipitation systems. Rev. Geophys., 27: 345–370.

Chan, S.-O. and Bras, R.L., 1979. Urban storm water management: Distribution of flood volumes. Water Resour. Res., 15: 371–382.

Cho, H.-R., 1985. Stochastic dynamics of precipitation. Water Resour. Res., 21: 1225–1232.

Crane, R.K., 1990. Space–time structure of rain rate fields. J. Geophys. Res., 95: 2011–2020.

Felgate, D.G. and Read, D.G., 1975. Correlation analysis of the cellular structure of storms observed by raingauges. J. Hydrol., 24: 191–200.

Gupta, V.K., 1985. Preface for special section on investigation of mesoscale precipitation fields. Water Resour. Res., 21: 1223–1225.

Gupta, V.K. and Waymire, E.C., 1979. A stochastic kinematic study of subsynoptic space–time rainfall. Water Resour. Res., 15: 637–644.

Hershfield, D.M., 1962. Extreme rainfall relationships. J. Hydraul. Div., Proc. ASCE, HY6: 73–79.

Hobbs, P.V. and Locatelli, J.D., 1978. Rainbands, precipitation cores and generating cells in a cyclonic storm. J. Atmos. Sci., 35: 230–241.

Huff, F.A. and Shipp, W.L., 1969. Spatial correlations of storm, monthly and seasonal precipitation. J. Appl. Meteorol., 8: 542–550.

Jinno, K., Kawamura, A., Berndtsson, R., Larson, M. and Niemczynowicz, J., 1993. Real-time rainfall prediction at urban space–time scales using a two-dimensional stochastic advection–diffusion model. Water Resour. Res., 29: 1489–1504.

Marshall, R.J., 1980. The estimation and distribution of storm movement and storm structures, using a correlation analysis technique and rain-gage data. J. Hydrol., 48: 19–31.

Messaoud, M. and Pointin, Y.B., 1990. Small time and space measurements of the mean rainfall rate made by a gage network and by a dual-polarization radar. J. Appl. Meteorol., 29: 830–841.

Niemczynowicz, J., 1984. An investigation of the areal and dynamic properties of short-term rainfall and its influence on runoff generating processes. Dissertation, Rep. 1005, Department of Water Research Engineering, Lund Inst. Sci. Technol., University of Lund, Lund, pp. 1–215.

Niemczynowicz, J., 1987. Storm tracking using raingauge data. J. Hydrol., 93: 135–152.

Niemczynowicz, J. and Dahlblom, P., 1984. Dynamic properties of rainfall in Lund. Nord. Hydrol., 15: 9–24.

Niemczynowicz, J. and Jönsson, O., 1981. Extreme rainfall events in Lund 1979–80. Nord. Hydrol., 12: 129–142.

Orlanski, I., 1975. A rational subdivision of scales for atmospheric processes. Bull. Am. Meteorol. Soc., 6: 527–530.

Panofsky, H.A. and Dutton, J.A., 1984. Atmospheric Turbulence. Wiley, New York.

Schilling, W., 1990. Rainfall data for urban hydrology: What do we need? In: J. Niemczynowicz (Editor), Proc. Int. Workshop on Urban Rainfall and Meteorology, St. Moritz, Switzerland, 2–5 December 1990, University of Lund, Lund, pp. 13–38.

Sharon, D., 1972. The spottiness of rainfall in a desert area. J. Hydrol., 17: 161–175.

Sharon, D., 1974. The spatial pattern of convective rainfall in Sukumaland, Tanzania — a statistical analysis. Arch. Meteorol. Geophys. Bioklim., 22B: 201–218.

Shaw, S.R., 1983. An investigation of the cellular structure of storms using correlation techniques. J. Hydrol., 62: 63–79.

Taylor, G.I., 1938. The spectrum of turbulence. Proc. R. Soc. London, Ser. A., 164: 476–490.

Yen, B.C., 1987. Urban drainage hydraulics and hydrology: from art to science. In: B.C. Yen (Editor), Urban Drain, Hydraulics and Hydrology, Proc. Fourth Int. Conf. Urban Storm Drainage, Lausanne, 31 August–4 September, 1987. IAHR, Lausanne, pp. 1–24.

Yevjevich, V., 1972. Stochastic processes in hydrology. Water Resources, Fort Collins, CO, pp. 1–276.

Zawadzki, I.I., 1973. Statistical properties of precipitation patterns. J. Appl. Meteorol., 12: 459–472.